Spatial Multiplexing of Atom-Photon Entanglement Sources using Feedforward Control and Switching Networks

Long Tian, Zhongxiao Xu, Lirong Chen, Wei Ge, Haoxiang Yuan, Yafei Wen, Shengzhi Wang, Shujing Li, and Hai Wang*
The State Key Laboratory of Quantum Optics and Quantum Optics Devices, Collaborative Innovation Center of Extreme Optics, Institute of Opto-Electronics, Shanxi University, Taiyuan 030006, People's Republic of China
(Received 26 December 2016; published 29 September 2017)

The light-matter quantum interface that can create quantum correlations or entanglement between a photon and one atomic collective excitation is a fundamental building block for a quantum repeater. The intrinsic limit is that the probability of preparing such nonclassical atom-photon correlations has to be kept low in order to suppress multiexcitation. To enhance this probability without introducing multiexcitation errors, a promising scheme is to apply multimode memories to the interface. Significant progress has been made in temporal, spectral, and spatial multiplexing memories, but the enhanced probability for generating the entangled atom-photon pair has not been experimentally realized. Here, by using six spin-wave-photon entanglement sources, a switching network, and feedforward control, we build a multiplexed light-matter interface and then demonstrate a ∼sixfold (∼fourfold) probability increase in generating entangled atom-photon (photon-photon) pairs. The measured compositive Bell parameter for the multiplexed interface is 2.49 ± 0.03 combined with a memory lifetime of up to ∼51 μs.

DOI: 10.1103/PhysRevLett.119.130505

The distribution of entanglement over a long distance is a central task of quantum communication [1–5]. Because of transmission losses in optical fibers, directly distributing entanglement over long distance (>500 km) is limited [6–8]. To overcome this limitation, Briegel *et al.* proposed a quantum repeater (QR) protocol [9], in which the entanglement distance between two locations is divided into N shorter elementary links. Entanglement is generated in each link and then successively extended via entanglement swapping between two adjacent links. To realize a practical QR, an attractive approach is the Duan, Lukin, Cirac, and Zoller (DLCZ) protocol [3], which uses atomic ensembles as memory elements and single-photon detection for entanglement creation and swapping. Based on the DLCZ protocol, several improved QR schemes have been proposed [10–15], in which a robust QR scheme [10,11] has been paid more attention. In this scheme, entanglement swapping and connection are achieved by using two-photon detection; thereby the long-distance phase stability, required in DLCZ protocol, is no longer necessary [1]. The fundamental building block for the DLCZ-type or robust QR protocols [1,10,11] is a light-mater quantum interface (LMQI) that can generate entanglement between a photon and an atomic collective excitation in a probabilistic way. Such LMQIs have been experimentally demonstrated by using spontaneous Raman scattering in cold atomic ensembles [16–30], or storing one of the correlated or entangled photons in a solid-state [31–34] or gas-state atomic ensemble [35]. Additionally, entanglement between a single photon and a single quantum system such as a nitrogen-vacancy center [36], or a trapped atom or ion [37–41], has been experimentally demonstrated and proposed for alternative QR approaches [42–45]. The atomic-ensemble-based LMQIs [16–35] are attractive because they use relatively simple ingredients [1,14]. However, the probability to prepare the atom-photon entanglement in such LMQIs has to be kept low for avoiding multiexcitation errors. So, the entanglement distribution over a long distance requires a long storage time; e.g., 1000 km entanglement distribution requires a time of 10-second order, which exceeds the state-of-the-art results [21]. For greatly reducing the required time, the multiplexed QR protocols are proposed [46,47], in which the temporally or spatially multiplexed memories are introduced into the atomic-ensemble-based LMQI and the generation probability of atom-photon correlation or entanglement pairs is greatly enhanced [1,46,47]. In recent years, many multimode-memory experiments, including storage of five temporally multiplexed polarization qubits [48] and 26 spectrally multiplexed time-bin qubits [49] at the single-photon level, as well as 50 temporally multiplexed light pulses [50], have been demonstrated. It is worth noting that the authors in Ref. [49] utilized feedforward-controlled operations on the retrieved qubits encoded into the multiplexed spectral modes. The LMQIs with six spectral modes [51], and with 12 independently addressable spatial-mode memories [52], have been demonstrated and the atom-photon correlation and entanglement were observed in the two experiments, respectively. Recently, Tiranov *et al.* demonstrated and certified the simultaneous storage and retrieval of two entangled photons inside a solid-state quantum memory [53]. However, the enhanced preparation rate for the atom-photon correlated or entangled pair has not been observed in these experiments due to lack of the feedforward-controlled write (storing) [52] or read (retrieving) [51,53] process.

Here, we demonstrate a multiplexed light-matter-entanglement interface (LMEI) formed by a spatial array consisting of six spin-wave-photon entanglement (SWPE) sources together with a feedforward-controlled optical switching network (OSN) and then achieve a sixfold (fourfold) enhancement of the atom-photon (photon-photon) entanglement generation probability without introducing extra noise. In addition, also the compositive fidelity (Bell parameter) is used for characterizing the quality of the entanglement created in the multiplexed LMEI, whose measured maximal value is $87.9\% \pm 1\%$ (2.49 ± 0.03), overcoming the critical limit of 78% [54]. In contrast to the previous spatially multiplexed schemes [47,52,55], where multiple independent subensembles are used as memory elements, our presented scheme uses only multiple spatial modes in an ensemble as memory elements.

We now show that our multiplexed LMEI is available for the QR protocol shown in Fig. 1, where, m SWPE sources generated from an atomic ensemble are located at the end point of each elementary link (i.e., node). In an elementary link, e.g., A-B link in Fig. 1(a), a single photon coming from the ith source located at the left (A) ensemble is sent to the ith central station (CS_i) of the link to meet another photon coming from the ith source from the right (B) ensemble. At each of the stations CS_i $(i = 1, ..., m)$, the two photons undergo a Bell-state measurement (BSM) behind a polarization-beam splitter (PBS). A successful BSM, e.g., at the kth station (CS_k), indicates that an entangled state between two spin-wave qubits, which are stored in kth spatial modes of the left and right ensembles, respectively, is created; i.e., entanglement between the two ensembles is established. For performing the entanglement swapping between the A-B and C-D links [Fig. 1(b)], one converts the spin-wave excitations stored in the B and C ensembles into two anti-Stokes photons, respectively, and combines them on a PBS. Since the retrieved photon from the B (C) ensemble may come from any of the spatial modes, one has to route it into a common channel (see Sec. IV in Supplemental Material [56] for details) to achieve this swapping.

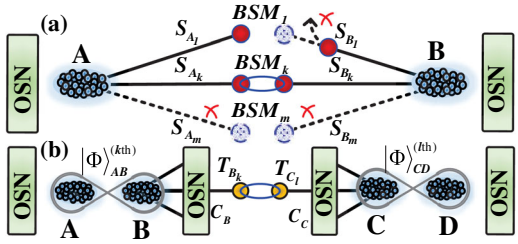

FIG. 1. Quantum repeater scheme based on the multiplexed interfaces. (a) Entanglement creation in an elementary link. A and B ensembles are located at the left and right end points of the link, respectively. Each one is synchronically excited by write-laser pulses, which generates m SWPE sources, labeled by $|\Phi\rangle_{A(B)}^{(1\mathrm{st})}, \ldots, |\Phi\rangle_{A(B)}^{(i\mathrm{th})}, \ldots, |\Phi\rangle_{A(B)}^{(m\mathrm{th})}$. The SWPE source $|\Phi\rangle_{A}^{(i\mathrm{th})}$ $[|\Phi\rangle_{B}^{(i\mathrm{th})}]$ emits a Stokes photon $S_{A_i}(S_{B_i})$ and creates one spin-wave excitation $M_{A_i}(M_{B_i})$. The photons S_{A_i} and S_{B_i} are sent to the ith middle station between A and B ensembles for the BSM. Conditioned on a successful BSM at the kth station, for example, the ensembles A and B are projected into an entangled state $|\Phi\rangle_{AB}^{(k\mathrm{th})}$. (b) Entanglement swapping between two adjacent links. The ensemble C (D) also creates m SWPE sources and a successful BSM at the lth central station of the C-D link, e.g., projects the C and D ensembles into an entangled state $|\Phi\rangle_{CD}^{(l\mathrm{th})}$. To performing an entanglement swapping between the A-B and C-D links, we convert the spin-wave excitation $M_{B_k}(M_{C_l})$ into an anti-Stokes photon $T_{B_k}(T_{C_l})$ and route it into a common channel $C_B(C_C)$ by using a feedforward-controlled OSN.

Aiming at the above multiplexed QR scheme, we experimentally demonstrate a multiplexed interface (MI) by using six SWPE sources in a single atomic ensemble utilizing feedforward control. The experimental setup and relevant atomic levels are shown in Fig. 2. The atomic ensemble is a cloud of cold ^{87}Rb atoms, whose two ground levels $|a\rangle$ and $|b\rangle$, together with the excited level $|e_1\rangle$ ($|e_2\rangle$), form a Λ-type configuration. The atoms are prepared in the initial state $|a\rangle$ and then an off-resonant σ^+-polarized writing pulse is applied to them along the z axis. The writing pulses induce the Raman transition $|a\rangle \rightarrow |b\rangle$ via $|e_1\rangle$ [Fig. 2(b)], which emits Stokes photons and simultaneously creates spin-wave

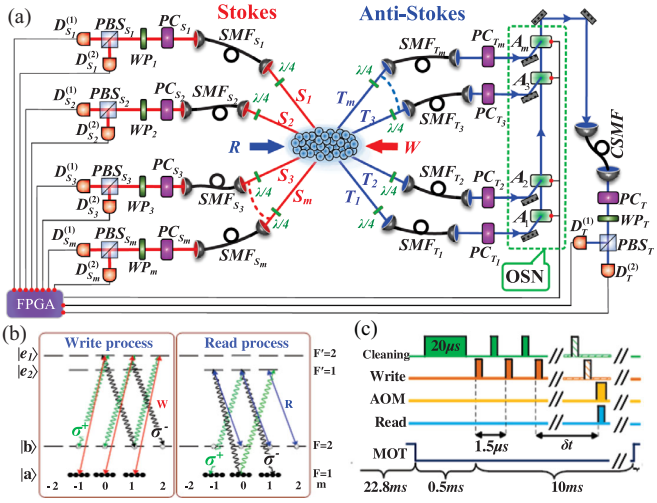

FIG. 2. Overview of the experiment. (a) Experiment setup for the 6-SWPE sources in combination with feedforward control (Noted that we only plot 4-SWPE sources in the figure). PC. phase compensator (see Sec. II in Supplemental Material [56]); $A_{(1,2,\ldots,6)}$. acousto-optic modulators; $\mathrm{WP}_{1,2,\ldots,6,T}$. half-wave or quarter-wave plates. In the measurements of the fidelities (Fig. 5) or polarization visibilities (Fig. 3), the $\mathrm{WP}_{1,2,\ldots,6,T}$ are half-wave (quarter-wave) plates when analyzing the photon polarization in the D or A (R or L) polarization setting and are removed when analyzing the photon polarization in H or V polarization setting (see Sec. V in Supplemental Material [56]). In the measurements of the Bell parameter, the $\mathrm{WP}_{1,2,\ldots,6,T}$ are half-wave plates and used for setting the polarization angles. (b) Relevant atomic levels. (c) Time sequence of an experimental cycle.

excitations. We collect the Stokes photons in different spatial modes $S_i (i = 1, ..., 6)$ at small angles relative to the z axis. If a single Stokes photon is emitted in the spatial mode S_i, one atomic spin-wave excitation is created and stored in the spatial mode M_i, with the wave vector $k_{M_i} = k_W - k_{S_i}$, where k_W and k_{S_i} are the wave vectors of the write and Stokes fields, respectively. The atom-photon system can be written as [23,29] $\rho_{ap}^{(i\text{th})} = |0\rangle\langle 0| + \chi_i |\Phi\rangle^{(i\text{th})\,(i\text{th})}\langle\Phi|$, where $|\Phi\rangle^{(i\text{th})} = \sqrt{\chi_i}(\cos\vartheta|+\rangle_{M_i}|R\rangle_{S_i} + \sin\vartheta|-\rangle_{M_i}|L\rangle_{S_i})$ is the ith spin-wave-photon entangled state, $|+\rangle_{M_i}$ ($|-\rangle_{M_i}$) represents one spin-wave excitation associated with Zeeman coherence $|a, m_a\rangle \leftrightarrow |b, m_b = m_a\rangle$ ($|a, m_a\rangle \leftrightarrow |b, m_b = m_a + 2\rangle$), $|R\rangle_{S_i}$ ($|L\rangle_{S_i}$) denotes a $\sigma^+(\sigma^-)$-polarized Stokes photon, and $\cos\vartheta$ is the relevant Clebsch-Gordan coefficient [23]. In the presented experiment, we transform the $\sigma^+(\sigma^-)$ polarization of the Stokes photon S_i into the H-V polarization by using a $\lambda/4$ plate. The Stokes photon S_i is collected by a single-mode fiber (SMF_{S_i}), and then guided to a polarization-beam splitter (PBS_{S_i}) that transmits horizontal (H) polarization into detector $D_{S_i}^{(1)}$ and reflects vertical (V) polarization into detector $D_{S_i}^{(2)}$. The detection events at the detectors $D_{S_i} (i = 1, ..., 6)$ are processed by a field programmable gate array (FPGA) for further analysis. Once a photon is detected by the ith detector D_{S_i}(either $D_{S_i}^{(1)}$ or $D_{S_i}^{(2)}$), one spin-wave excitation has been heralded to be stored in the mode M_i and the subsequent write sequence is stopped by the feedforward signal from the FPGA. After a storage time δt, a reading laser pulse is applied to convert the spin-wave excitation M_i into the anti-Stokes photon T_i. By using a $\lambda/4$ plate, we transform the $\sigma^+(\sigma^-)$ polarization of the photon T_i into the H-V polarization. So, the atom-photon state is transformed into the entangled two-photon state $|\Phi\rangle'^{(i\text{th})}_{S,T} = (\cos\vartheta|H\rangle_{T_i}|H\rangle_{S_i} + \sin\vartheta|V\rangle_{T_i}|V\rangle_{S_i})$.

The photon T_i passes through the single-mode fiber SMF_{T_i} and is sent to ith input port of an $m \times 1$ OSN. Based on the feedforward-controlled signal, the OSN routes the T_i photon into a common single-mode fiber (CSMF). Passing through the CSMF, the photon T_i impinges on a polarization-beam splitter (PBS_T), which transmits an H-polarized photon (reflects an V-polarized photon) to detector $D_T^{(1)}$ [$D_T^{(2)}$].

The preparation rate of the atom-photon (photon-photon) entanglement pair can be evaluated by the rate of detected Stokes photons (coincidence count) in the H-V polarization setting. For the nonmultiplexed case, in which only one source, for example, the ith source, is operating, the Stokes detection (coincidence count) rate for the source is given by $R_{H\text{-}V}^{(i\text{th})} = r\{p_{SH}^{(i\text{th})} + p_{SV}^{(i\text{th})}\}$ ($C_{H\text{-}V}^{(i\text{th})} = C_{SH,TH}^{(i\text{th})} + C_{SV,TV}^{(i\text{th})}$), where r is the repetition rate, $p_{SH}^{(i\text{th})}$ ($p_{SV}^{(i\text{th})}$) is the probability of detecting a photon at the detector $D_{S_i}^{(1)}$ ($D_{S_i}^{(2)}$), and $C_{SH,TH}^{(i\text{th})}$ ($C_{SV,TV}^{(i\text{th})}$) is the coincidence count rate between the detectors $D_{S_i}^{(1)}$ ($D_{S_i}^{(2)}$) and $D_T^{(1)}$ ($D_T^{(2)}$). For the multiplexed case, m SWPE sources are simultaneously excited and the OSN is used for routing the anti-Stokes photons. In this case, the total Stokes detection (coincidence count) rate is written as $R_{H\text{-}V}^{(m)} = r\sum_{i=1}^{m}\{p_{SH}^{(M,i\text{th})} + p_{SV}^{(M,i\text{th})}\}$ ($C_{H\text{-}V}^{(m)} = \sum_{i=1}^{m} C_{H\text{-}V}^{(M,i\text{th})} = \sum_{i=1}^{m}\{C_{SH,TH}^{(M,i\text{th})} + C_{SV,TV}^{(M,i\text{th})}\}$), where $p_{SH}^{(M,i\text{th})}$ ($p_{SV}^{(M,i\text{th})}$) is the probability of detecting a photon at the detector $D_{S_i}^{(1)}$ ($D_{S_i}^{(2)}$), $C_{SH,TH}^{(M,i\text{th})}$ ($C_{SV,TV}^{(M,i\text{th})}$) is the coincidence count rate between the detectors $D_{S_i}^{(1)}$ ($D_{S_i}^{(2)}$) and $D_T^{(1)}$ ($D_T^{(2)}$), and the superscript M denotes the multiplexed case.

To verify that the MI can enhance the probability for generating entangled atom-photon (photon-photon) pairs while introducing no extra noise, we measure the polarization visibilities versus the Stokes detection (coincidence count) rate for the multiplexed and nonmultiplexed case. For the nonmultiplexed case, the polarization visibility of the two photons from the source i in the H-V polarization setting is defined as $V_{H\text{-}V}^{(i\text{th})} = (C_{H\text{-}V}^{(i\text{th})} - N_{H\text{-}V}^{(i\text{th})})/(C_{H\text{-}V}^{(i\text{th})} + N_{H\text{-}V}^{(i\text{th})})$, where $C_{H\text{-}V}^{(i\text{th})} = C_{SH,TH}^{(i\text{th})} + C_{SV,TV}^{(i\text{th})}$ ($N_{H\text{-}V}^{(i\text{th})} = C_{SH,TV}^{(i\text{th})} + C_{SV,TH}^{(i\text{th})}$) denotes the coincidence count rate, which is measured when the router circuitry consisting of OSN and CSMF is removed. For the multiplexed case, the polarization visibility of the entangled two photons from the MI in the H-V basis is defined as [see Eq. (S37) in Supplemental Material [56]] $V_{H\text{-}V}^{(M)} = \sum_{i=1}^{m=6} P_{S,T}^{(M,i\text{th})} V_{H\text{-}V}^{(M,i\text{th})} \approx (C_{H\text{-}V}^{(m)} - N_{H\text{-}V}^{(m)})/(C_{H\text{-}V}^{(m)} + N_{H\text{-}V}^{(m)})$, where $N_{H\text{-}V}^{(m)} = \sum_{i=1}^{m} N_{H\text{-}V}^{(M,i\text{th})} = \sum_{i=1}^{m}(C_{SH,TV}^{(M,i\text{th})} + C_{SV,TH}^{(M,i\text{th})})$, $P_{S,T}^{(M,i\text{th})} = (C_{H\text{-}V}^{(M,i\text{th})} + N_{H\text{-}V}^{(M,i\text{th})})/(C_{H\text{-}V}^{(m)} + N_{H\text{-}V}^{(m)})$ represents the normalized coincidence probability, and $C_{SH,TV}^{(M,i\text{th})}$ ($C_{SV,TH}^{(M,i\text{th})}$) is the coincidence count rate between the detectors $D_{S_i}^{(1)}$ ($D_{S_i}^{(2)}$) and $D_T^{(2)}$ ($D_T^{(1)}$).

Before showing the visibilities as a function of the Stokes detection (coincidence count) rates, we measured the two-photon coincidences of the MI in H-V, D-$A = +45°(-45°)$ and R-L polarization settings for a fixed value of $p_S^{(m=6)} \approx 1.26\%$, where $p_S^{(m=6)} = \sum_{i=1}^{m=6} p_S^{(M,i\text{th})}$ is the total Stokes-detection probability, with $p_S^{(M,i\text{th})}$ being the probability detecting a photon at the detector D_{S_i}(either $D_{S_i}^{(1)}$ or $D_{S_i}^{(2)}$) for the multiplexed case. The measured results are plotted in the histogram shown in Fig. 3. From the results, we calculated the visibilities of the MI for H-V, D-A, and R-L polarization settings according to Eq. (S37) in Supplemental Material, which are $V_{H\text{-}V}^{(M)} \approx 94.1\%$, $V_{D\text{-}A}^{(M)} \approx 84.4\%$, and $V_{R\text{-}L}^{(M)} \approx 81.6\%$, respectively.

The red, yellow, pink, green, blue, and purple data in Figs. 4(a) and 4(b) are the measured polarization visibilities $V_{H\text{-}V}^{(1\text{st})}$, $V_{H\text{-}V}^{(2\text{nd})}$, and $V_{H\text{-}V}^{(6\text{th})}$ as the functions of the Stokes detection (coincidence count) rate in the H-V polarization

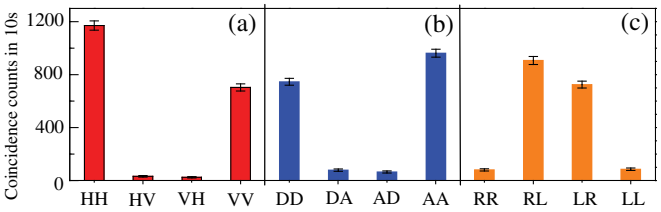

FIG. 3. Coincidences between the Stokes and anti-Stokes photons from the multiplexed LMEI at (a) H-V, (b) D-A, and (c) R-L polarization settings for $p_S^{(m=6)} \approx 1.26\%$ and $\delta t = 1\ \mu$s. Error bars represent ± 1 standard deviation.

setting for the individual sources 1,2,…,6, respectively, which are measured under the nonmultiplexed case. The black data in Figs. 4(a) and 4(b) are the measured visibilities for the MI versus $R_{H\text{-}V}^{(m)}$ and $C_{H\text{-}V}^{(m)}$, respectively. The blue (red) solid lines in Figs. 4(a) and 4(b) are the linear fittings to the single-source data (multiplexed data $V_{H\text{-}V}^{(M)}$). In the measurements, we fix the storage time at $\delta t = 1\ \mu$s and increase the Stokes-detection (coincidence count) rates by increasing the write-light power. As shown in Figs. 4(a) and 4(b), the polarization visibilities $V_{H\text{-}V}^{(\mathrm{ith})}$ $(i = 1, 2, ..., 6)$ and $V_{H\text{-}V}^{(M)}$ decrease with the increase in the Stokes-detection (coincidence count) rates due to multiexcitation noise. However, for a fixed visibility, the MI gives rise to a 5.94-fold (3.98-fold) increase in the Stokes detection rate (coincidence count rate) compared to the nonmultiplexed interface. These results agree with the theoretical prediction of $m = 6$ ($\bar{\eta}_{RC} \times m \approx 4.1$) based on Eq. (S57) [Eq. (S59)] in Supplemental Material [56], indicating that the application of the router circuitry controlled by the feedforward control does not introduce extra noise. Similarly to the measurements in Fig. 4, we also measure the dependences of the visibilities on the Stokes detection (coincidence count) rates in D-$A = +45°(-45°)$ and R-L polarization settings. The measured

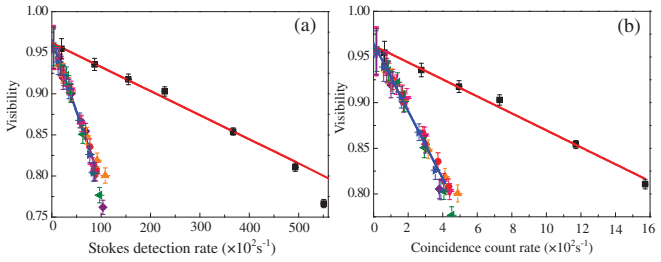

FIG. 4. The polarization visibility as functions of Stokes detection rate (a) and coincidence count rate (b) for the polarization setting of H-V, respectively. The blue solid lines in (a) and (b) are the least-square fittings to the single-source data according to Eqs. (S48) and (S49) in Supplemental Material [56], respectively, while the red solid lines in (a) and (b) are the least-square fittings to the multiplexed data $V_{H\text{-}V}^{(M)}$ according to Eqs. (S57) and (S59) in Supplemental Material [56], respectively.

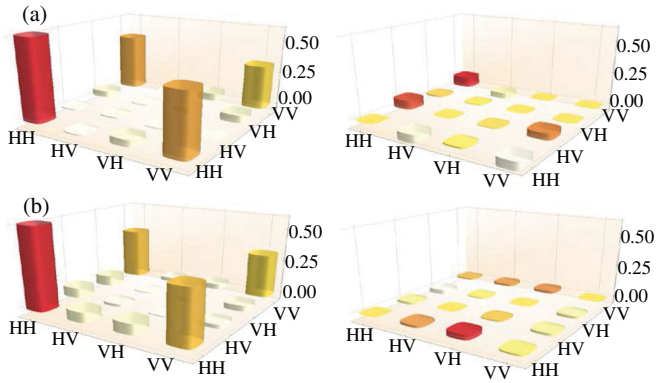

FIG. 5. Real and imaginary parts of the reconstructed density matrices $\rho_r^{(M,1\mathrm{st})}$ and $\rho_r^{(M,3\mathrm{rd})}$ of the two photons from the sources 1(a) and 3(b), respectively.

results are shown in Figs. S1 and S2 in Supplemental Material [56], which show that the MI enables a ~5.9-fold (~3.9-fold) increase in the probability of generating entangled atom-photon (photon-photon) pairs without introducing extra noise.

The quality of the created entanglement in the MI can be characterized by the compositive fidelity, which is defined by $F^{(M)} \approx \sum_{i=1}^{m=6} P_{S,T}^{(M,\mathrm{ith})} F^{(M,\mathrm{ith})}$ [see Eq. (S2) in Supplemental Material [56]], where $P_{S,T}^{(M,\mathrm{ith})} = p_{S,T}^{(M,\mathrm{ith})} / \sum_{i=1}^{m} p_{S,T}^{(M,\mathrm{ith})}$, $p_{S,T}^{(M,\mathrm{ith})}$ is the coincidence probability between the detectors D_{S_i} (either $D_{S_i}^{(1)}$ or $D_{S_i}^{(2)}$) and D_T (either $D_T^{(1)}$ or $D_T^{(2)}$), $F^{(M,\mathrm{ith})} = \left(\mathrm{Tr}\sqrt{\sqrt{\rho_r^{(M,\mathrm{ith})}}\rho_d\sqrt{\rho_r^{(M,\mathrm{ith})}}}\right)^2$, $\rho_r^{(M,\mathrm{ith})}$ is the reconstructed density matrix of the ith entangled atom-photon state, and ρ_d is the density matrix of the entangled state defined by $|\Phi\rangle_{S,T}^{\prime(\mathrm{ith})}$. The probability $P_{S,T}^{(M,\mathrm{ith})}$ and fidelities $F^{(M,\mathrm{ith})}$ ($i = 1$ to 6) are directly measured under the multiplexed case. Figures 5(a) and 5(b) plot the reconstructed density matrices $\rho_r^{(M,1\mathrm{st})}$ and $\rho_r^{(M,3\mathrm{rd})}$, respectively, which yield $F^{(M,1\mathrm{st})} = 87.1\%$ and $F^{(M,3\mathrm{rd})} = 88.0\%$. Table I shows the measured $F^{(M)}$ for several different values of $p_S^{(m=6)}$ for a delay time of 1 μs. For $p_S^{(6)} \approx 1.26\%$ corresponding to the write-light power to obtain $C_{H\text{-}V}^{(6)} \approx 200\ \mathrm{s}^{-1}$ (see Fig. 4), we measure a maximal fidelity of $F^{(M)} = 87.9\%$.

TABLE I. Measurement of the fidelity $F^{(M)}$ and Bell parameter $S^{(M)}$ for several different values of the total-Stokes-detection probability $p_S^{(6)}$ at $\delta t = 1\ \mu$s. Error bars represent ± 1 standard deviation.

$p_S^{(6)}$	0.0126	0.0297	0.0421	0.0594	0.0738
$F^{(M)}$	0.87(1)	0.85(1)	0.82(1)	0.78(1)	0.75(1)
$S^{(M)}$	2.49(3)	2.38(1)	2.29(2)	2.17(2)	2.09(2)

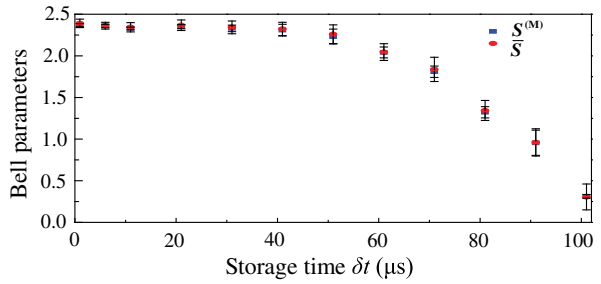

FIG. 6. Measurements of the Bell parameters $S^{(M)}$ and $\bar{S}$ as a function of δt for $p_S^{(6)}=0.0297$. Error bars represent ± 1 standard deviation.

The quality of the entangled atom-photon states created in the MI can also be described by a compositive Bell parameter $S^{(M)}$, which is defined as [see Eq. (S105) in Supplemental Material [56]] $S^{(M)}=\sum_{i=1}^{m=6} P_{S,T}^{(M,i\mathrm{th})} S^{(M,i\mathrm{th})} = |E^{(M)}(\theta_{S_i},\theta_T)-E^{(M)}(\theta_{S_i},\theta'_T)+E^{(M)}(\theta'_{S_i},\theta_T)+E^{(M)}(\theta'_{S_i},\theta'_T)|<2$, where $S^{(M,i\mathrm{th})}$ is the Bell parameter between the photons S_i and T_i, θ_{S_i} (θ_T) is the polarization angle of the Stokes (anti-Stokes) field, which is set by rotating a $\lambda/2$ plate before PBS_{S_i} (PBS_T), and $E^{(M)}(\theta_{S_i},\theta_T)$ is the correlation function defined by

$$\frac{\sum_{i=1}^{m}\left[C_{SH,TH}^{(M,i\mathrm{th})}(\theta_{S_i},\theta_T)+C_{SV,TV}^{(M,i\mathrm{th})}(\theta_{S_i},\theta_T)-C_{SH,TV}^{(M,i\mathrm{th})}(\theta_{S_i},\theta_T)-C_{SV,TH}^{(M,i\mathrm{th})}(\theta_{S_i},\theta_T)\right]}{\sum_{i=1}^{m}\left[C_{SH,TH}^{(M,i\mathrm{th})}(\theta_{S_i},\theta_T)+C_{SV,TV}^{(M,i\mathrm{th})}(\theta_{S_i},\theta_T)+C_{SH,TV}^{(M,i\mathrm{th})}(\theta_{S_i},\theta_T)+C_{SV,TH}^{(M,i\mathrm{th})}(\theta_{S_i},\theta_T)\right]}; \quad (1)$$

for example, $C_{SH,TH}^{(M,i\mathrm{th})}(\theta_{S_i},\theta_T)$ [$C_{SV,TV}^{(M,i\mathrm{th})}(\theta_{S_i},\theta_T)$] is the coincidence detection rate between the detectors $D_{S_i}^{(1)}$ [$D_{S_i}^{(2)}$] and $D_T^{(1)}$ [$D_T^{(2)}$] for the polarization angle θ_{S_i} and θ_T. In the measurement, the canonical settings are chosen to be $\theta_{S_i}=0°$, $\theta'_{S_i}=45°$ ($i=1$ to 6), $\theta_T=22.5°$ and $\theta'_T=67.5°$. Table I also shows the measured data of $S^{(M)}$ for several different values of $p_S^{(6)}$ when $\delta t=1$ μs. For $p_S^{(6)}\approx 0.0126$, we achieve a maximal value of $S^{(M)}=2.49\pm 0.03$, violating Bell–Clauser-Horne-Shimony-Holt (CHSH) inequality by ~16 standard deviations.

To investigate the ability to use the atomic ensemble for quantum memory applications, we measure the decay of the Bell parameter $S^{(M)}$ with the storage time δt. In the measurements, the peak power of write pulse is fixed to get $p_S^{(6)}=0.0297$ (corresponding to $C_{H\text{-}V}^{(6)}\approx 400\ \mathrm{s}^{-1}$). The blue square dots in Fig. 6 depict the measured $S^{(M)}$ data, which show that even after storing the spin-wave excitation for 51 μs, violates the corresponding CHSH inequality by 2.9 standard deviations ($S^{(M)}=2.23\pm 0.08$). The red circle dots are the average Bell parameter defined by $\bar{S}=(S^{(M,1\mathrm{st})}+S^{(M,2\mathrm{nd})}+,\ldots,+S^{(M,m\mathrm{th})})/m$, which is consistent with the values of $S^{(M)}$, indicating that the six SWPE sources are approximately symmetric in the detection and retrieval efficiency [see Eq. (S111) in Supplemental Material [56]].

In summary, a key advance of our demonstrated multiplexed LMEI is the enhanced rate for generating entangled atom-photon (photon-photon) pairs without introducing additional noise. Several criteria such as compositive visibility, fidelity, and Bell parameter are applied for judging the quality of the entanglement created in the MI. The transmission of the OSN remains unchanged when the multimode number scales up. To apply such multiplexed LMEI into long-distance QR applications, its several quantities need to be further improved. The lower retrieval efficiency (~15%) can be increased by using the high optical-depth cold atoms or coupling the atoms into an optical cavity [21]. The short storage lifetime (~51 μs) can be extended by trapping atoms in an optical lattice [21] and selecting two magnetic-field-insensitive spin waves to store memory qubits [63]. The low multimode number can be further extended by collecting Stokes photons at more directions [64,65]. When the presented spatially multiplexed scheme is combined with temporally multiplexed storage approaches [66–69], one could achieve a multiplexing of a large number of modes, which will significantly improve entanglement distribution rates in long-distance quantum communications.

The authors are grateful to the referees for constructive and helpful suggestions. We also thank Professor Jing Zhang for helpful suggestions. We acknowledge funding support from Key Project of the Ministry of Science and Technology of China (Grant No. 2016YFA0301402), the National Natural Science Foundation of China (Grants No. 11475109, No. 11274211, and No. 11604191), and the Program for Sanjin Scholars of Shanxi Province of China.

*wanghai@sxu.edu.cn

[1] N. Sangouard, C. Simon, H. de Riedmatten, and N. Gisin, Rev. Mod. Phys. **83**, 33 (2011).
[2] H. J. Kimble, Nature (London) **453**, 1023 (2008).
[3] L.-M. Duan, M. Lukin, J. I. Cirac, and P. Zoller, Nature (London) **414**, 413 (2001).
[4] A. I. Lvovsky, B. C. Sanders, and W. Tittel, Nat. Photonics **3**, 706 (2009).

[5] F. Bussières, N. Sangouard, M. Afzelius, H. de Riedmatten, C. Simon, and W. Tittel, J. Mod. Opt. **60**, 1519 (2013).
[6] B. Korzh, C. Ci Wen Lim, R. Houlmann, N. Gisin, M. J. Li, D. Nolan, B. Sanguinetti, R. Thew, and H. Zbinden, Nat. Photonics **9**, 163 (2015).
[7] N. Gisin, Front. Phys. **10**, 100307 (2015).
[8] H.-L. Yin, T.-Y. Chen, Z.-W. Yu, H. Liu, L.-X. You, Y.-H. Zhou, S.-J. Chen, Y. Mao, M.-Qi Huang, W.-J. Zhang, H. Chen, M. J. Li, D. Nolan, F. Zhou, X. Jiang, Z. Wang, Q. Zhang, X.-B. Wang, and J.-W. Pan, Phys. Rev. Lett. **117**, 190501 (2016).
[9] H. J. Briegel, W. Dür, J. I. Cirac, and P. Zoller, Phys. Rev. Lett. **81**, 5932 (1998).
[10] B. Zhao, Z. B. Chen, Y. A. Chen, J. Schmiedmayer, and J. W. Pan, Phys. Rev. Lett. **98**, 240502 (2007).
[11] Z.-B. Chen, B. Zhao, Y.-A. Chen, J. Schmiedmayer, and J.-W. Pan, Phys. Rev. A **76**, 022329 (2007).
[12] N. Sangouard, C. Simon, J. Minář, H. Zbinden, H. de Riedmatten, and N. Gisin, Phys. Rev. A **76**, 050301(R) (2007).
[13] J. Minář, H. de Riedmatten, and N. Sangouard, Phys. Rev. A **85**, 032313 (2012).
[14] N. Sangouard, C. Simon, B. Zhao, Y.-A. Chen, H. de Riedmatten, J.-W. Pan, and N. Gisin, Phys. Rev. A **77**, 062301 (2008).
[15] L. Jiang, J. M. Taylor, and M. D. Lukin, Phys. Rev. A **76**, 012301 (2007).
[16] B. Zhao, Y. A. Chen, X. H. Bao, T. Strassel, C. S. Chuu, X. M. Jin, J. Schmiedmayer, Z. S. Yuan, S. Chen, and J. W. Pan, Nat. Phys. **5**, 95 (2009).
[17] R. Zhao, Y. O. Dudin, S. D. Jenkins, C. J. Campbell, D. N. Matsukevich, T. A. B. Kennedy, and A. Kuzmich, Nat. Phys. **5**, 100 (2009).
[18] J. Simon, H. Tanji, J. K. Thompson, and V. Vuletić, Phys. Rev. Lett. **98**, 183601 (2007).
[19] T. Chaneliere, D. N. Matsukevich, S. D. Jenkins, S. Y. Lan, T. A. Kennedy, and A. Kuzmich, Nature (London) **438**, 833 (2005).
[20] A. G. Radnaev, Y. O. Dudin, R. Zhao, H. H. Jen, S. D. Jenkins, A. Kuzmich, and T. A. B. Kennedy, Nat. Phys. **6**, 894 (2010).
[21] S.-J. Yang, X.-J. Wang, X.-H. Bao, and J.-W. Pan, Nat. Photonics **10**, 381 (2016).
[22] C. W. Chou, H. de Riedmatten, D. Felinto, S. V. Polyakov, S. J. van Enk, and H. J. Kimble, Nature (London) **438**, 828 (2005).
[23] D. N. Matsukevich, T. Chaneliere, M. Bhattacharya, S. Y. Lan, S. D. Jenkins, T. A. B. Kennedy, and A. Kuzmich, Phys. Rev. Lett. **95**, 040405 (2005).
[24] D. N. Matsukevich, T. Chaneliere, S. D. Jenkins, S. Y. Lan, T. A. Kennedy, and A. Kuzmich, Phys. Rev. Lett. **96**, 030405 (2006).
[25] Y. O. Dudin, S. D. Jenkins, R. Zhao, D. N. Matsukevich, A. Kuzmich, and T. A. B. Kennedy, Phys. Rev. Lett. **103**, 020505 (2009).
[26] Y. O. Dudin, A. G. Radnaev, R. Zhao, J. Z. Blumoff, T. A. B. Kennedy, and A. Kuzmich, Phys. Rev. Lett. **105**, 260502 (2010).
[27] D.-S. Ding, W. Zhang, Z.-Y. Zhou, S. Shi, B.-S. Shi, and G.-C. Guo, Nat. Photonics **9**, 332 (2015).
[28] S. Chen, Y. A. Chen, B. Zhao, Z. S. Yuan, J. Schmiedmayer, and J. W. Pan, Phys. Rev. Lett. **99**, 180505 (2007).
[29] H. de Riedmatten, J. Laurat, C. W. Chou, E. W. Schomburg, D. Felinto, and H. J. Kimble, Phys. Rev. Lett. **97**, 113603 (2006).
[30] S. J. Yang, X. J. Wang, J. Li, J. Rui, X. H. Bao, and J. W. Pan, Phys. Rev. Lett. **114**, 210501 (2015).
[31] E. Saglamyurek, N. Sinclair, J. Jin, J. A. Slater, D. Oblak, F. Bussieres, M. George, R. Ricken, W. Sohler, and W. Tittel, Nature (London) **469**, 512 (2011).
[32] C. Clausen, I. Usmani, F. Bussieres, N. Sangouard, M. Afzelius, H. de Riedmatten, and N. Gisin, Nature (London) **469**, 508 (2011).
[33] E. Saglamyurek, J. Jin, V. B. Verma, M. D. Shaw, F. Marsili, S. W. Nam, D. Oblak, and W. Tittel, Nat. Photonics **9**, 83 (2015).
[34] F. Bussières, C. Clausen, A. Tiranov, B. Korzh, V. B. Verma, S. W. Nam, F. Marsili, A. Ferrier, P. Goldner, H. Herrmann, C. Silberhorn, W. Sohler, M. Afzelius, and N. Gisin, Nat. Photonics **8**, 775 (2014).
[35] H. Zhang, X.-M. Jin, J. Yang, H.-N. Dai, S.-J. Yang, T.-M. Zhao, J. Rui, Y. He, X. Jiang, F. Yang, G.-S. Pan, Z.-S. Yuan, Y. Deng, Z.-B. Chen, X.-H. Bao, S. Chen, B. Zhao, and J.-W. Pan, Nat. Photonics **5**, 628 (2011).
[36] B. Hensen, H. Bernien, A. E. Dreau, A. Reiserer, N. Kalb, M. S. Blok, J. Ruitenberg, R. F. L. Vermeulen, R. N. Schouten, C. Abellan, W. Amaya, V. Pruneri, M. W. Mitchell, M. Markham, D. J. Twitchen, D. Elkouss, S. Wehner, T. H. Taminiau, and R. Hanson, Nature (London) **526**, 682 (2015).
[37] J. Volz, M. Weber, D. Schlenk, W. Rosenfeld, J. Vrana, K. Saucke, C. Kurtsiefer, and H. Weinfurter, Phys. Rev. Lett. **96**, 030404 (2006).
[38] J. Hofmann, M. Krug, N. Ortegel, L. Gérard, M. Weber, W. Rosenfeld, and H. Weinfurter, Science **337**, 72 (2012).
[39] W. Rosenfeld, D. Burchardt, R. Garthoff, K. Redeker, N. Ortegel, M. Rau, and H. Weinfurter, arXiv:1611.04604.
[40] B. B. Blinov, D. L. Moehring, L. M. Duan, and C. Monroe, Nature (London) **428**, 153 (2004).
[41] D. L. Moehring, P. Maunz, S. Olmschenk, K. C. Younge, D. N. Matsukevich, L. M. Duan, and C. Monroe, Nature (London) **449**, 68 (2007).
[42] N. Sangouard, R. Dubessy, and C. Simon, Phys. Rev. A **79**, 042340 (2009).
[43] L. Childress, J. M. Taylor, A. S. Sørensen, and M. D. Lukin, Phys. Rev. Lett. **96**, 070504 (2006).
[44] P. van Loock, N. Lütkenhaus, W. J. Munro, and K. Nemoto, Phys. Rev. A **78**, 062319 (2008).
[45] C. Simon, Y. M. Niquet, X. Caillet, J. Eymery, J. P. Poizat, and J. M. Gerard, Phys. Rev. B **75**, 081302 (R) (2007).
[46] C. Simon, H. de Riedmatten, M. Afzelius, N. Sangouard, H. Zbinden, and N. Gisin, Phys. Rev. Lett. **98**, 190503 (2007).
[47] O. A. Collins, S. D. Jenkins, A. Kuzmich, and T. A. B. Kennedy, Phys. Rev. Lett. **98**, 060502 (2007).
[48] C. Laplane, P. Jobez, J. Etesse, N. Timoney, N. Gisin, and M. Afzelius, New J. Phys. **18**, 013006 (2015).
[49] N. Sinclair, E. Saglamyurek, H. Mallahzadeh, J. A. Slater, M. George, R. Ricken, M. P. Hedges, D. Oblak, C. Simon, W. Sohler, and W. Tittel, Phys. Rev. Lett. **113**, 053603 (2014).

[50] P. Jobez, N. Timoney, C. Laplane, J. Etesse, A. Ferrier, P. Goldner, N. Gisin, and M. Afzelius, Phys. Rev. A **93**, 032327 (2016).
[51] E. Saglamyurek, M. Grimau Puigibert, Q. Zhou, L. Giner, F. Marsili, V. B. Verma, S. Woo Nam, L. Oesterling, D. Nippa, D. Oblak, and W. Tittel, Nat. Commun. **7**, 11202 (2016).
[52] S.-Y. Lan, A. G. Radnaev, O. A. Collins, D. N. Matsukevich, T. A. B. Kennedy, and A. Kuzmich, Opt. Express **17**, 13639 (2009).
[53] A. Tiranov, P. C. Strassmann, J. Lavoie, N. Brunner, M. Huber, V. B. Verma, S. W. Nam, R. P. Mirin, A. E. Lita, F. Marsili, M. Afzelius, F. Bussières, and N. Gisin, Phys. Rev. Lett. **117**, 240506 (2016).
[54] M. Aspelmeyer, H. R. Böhm, T. Gyatso, T. Jennewein, R. Kaltenbaek, M. Lindenthal, G. Molina-Terriza, A. Poppe, K. Resch, M. Taraba, R. Ursin, P. Walther, and A. Zeilinger, Science **301**, 621 (2003).
[55] M. Razavi, M. Piani, and N. Lütkenhaus, Phys. Rev. A **80**, 032301 (2009).
[56] See Supplemental Material at http://link.aps.org/supplemental/10.1103/PhysRevLett.119.130505 for experimental details and calculations of polarization visibilities, fidelities, as well as the Bell parameter of the entangled state generated in the multiplexed interfaces, which includes Refs. [57–62].
[57] B. Albrecht, P. Farrera, X. Fernandez-Gonzalvo, M. Cristiani, and H. de Riedmatten, Nat. Commun. **5**, 3376 (2014).
[58] Y. Wu, L. Tian, Z. Xu, W. Ge, L. Chen, S. Li, H. Yuan, Y. Wen, H. Wang, C. Xie, and K. Peng, Phys. Rev. A **93**, 052327 (2016).
[59] J. W. Pan and A. Zeilinger, Phys. Rev. A **57**, 2208 (1998).
[60] S. Li, B. Wang, X. Yang, Y. Han, H. Wang, M. Xiao, and K. C. Peng, Phys. Rev. A **74**, 033821 (2006).
[61] Z. S. Yuan, Y. A. Chen, B. Zhao, S. Chen, J. Schmiedmayer, and J. W. Pan, Nature (London) **454**, 1098 (2008).
[62] I. Marcikic, H. de Riedmatten, W. Tittel, H. Zbinden, M. Legre, and N. Gisin, Phys. Rev. Lett. **93**, 180502 (2004).
[63] Z. X. Xu, Y. L. Wu, L. Tian, L. R. Chen, Z. Y. Zhang, Z. H. Yan, S. J. Li, H. Wang, C. D. Xie, and K. C. Peng, Phys. Rev. Lett. **111**, 240503 (2013).
[64] K. Surmacz, J. Nunn, K. Reim, K. C. Lee, V. O. Lorenz, B. Sussman, I. A. Walmsley, and D. Jaksch, Phys. Rev. A **78**, 033806 (2008).
[65] A. Grodecka-Grad, E. Zeuthen, and A. S. Sorensen, Phys. Rev. Lett. **109**, 133601 (2012).
[66] C. Simon, H. de Riedmatten, and M. Afzelius, Phys. Rev. A **82**, 010304 (2010).
[67] Q. Glorieux, J. B. Clark, A. M. Marino, Z. Zhou, and P. D. Lett, Opt. Express **20**, 12350 (2012).
[68] M. Hosseini, B. M. Sparkes, G. Campbell, P. K. Lam, and B. C. Buchler, Nat. Commun. **2**, 174 (2011).
[69] B. Albrecht, P. Farrera, G. Heinze, M. Cristiani, and H. de Riedmatten, Phys. Rev. Lett. **115**, 160501 (2015).